Novel Nanogels with Both Thermoresponsive and Hydrolytically Degradable Properties

Xiao Huang,[†,#] Gauri P. Misra,[†] Amit Vaish,[‡] John M. Flanagan,[||] Bryan Sutermaster,[‡] and Tao Lu Lowe*[,†,‡,⊥,§]

Departments of Surgery, Bioengineering, and Materials Science and Engineering, Pennsylvania State University, 500 University Drive, Hershey, Pennsylvania 17033

Received January 11, 2008; Revised Manuscript Received February 22, 2008

ABSTRACT: A series of novel nanogels with both thermoresponsive and hydrolytically degradable properties were synthesized by emulsion polymerization of *N*-isopropylacrylamide (NIPAAm) and dextran-lactate-2-hydroxyethyl methacrylate (DEXlactateHEMA), a hydrolytically degradable and cross-linkable dextran derivative, without using low molar mass surfactants. Various lengths of degradable oligolactate units and different precursor feeding ratios between NIPAAm and DEXlactateHEMA were used to synthesize the nanogels. FTIR measurements confirmed the chemical compositions and hydrolytic degradation of the synthesized nanogels. Dynamic light scattering measurements of the hydrodynamic radii of the nanogels in phosphate buffer saline (PBS, pH 7.4) against temperature and angle revealed that the nanogels were thermoresponsive with a lower critical solution temperature (LCST) of ∼32 °C. The size and morphology changes of the nanogels with degradation were investigated by using transmission electron microscopy, atomic force microscopy, and static light scattering techniques. AFM image analysis and Holtzer plots revealed that the nanogels became more rigid with degradation in water solutions.

Introduction

In recent years, there have been increasing research interests in designing micro- or nanoscaled polymer gels.[1–4] The reasons are that microgels or nanogels not only possess similar characteristics as their macroscopic counterparts—hydrogels, widely investigated for biomedical applications, membrane separation, and water treatment due to their unique 3-D network structure, biocompatibility, and exceptional physical and chemical properties—but also are superior to the macroscopic gels in terms of minimally invasive administration and increased patient compliance. Poly(*N*-isopropylacrylamide) (PNIPAAm) micro- and nanogels are the most widely studied micro- and nanogel systems because they can be easily synthesized in aqueous solution by emulsion polymerization,[5] and they also exhibit a reversible volume transition in water at ∼32 °C, defined as the lower critical solution temperature (LCST), so that they can be used to release drugs and catalyze reactions in response to temperature, pH, magnetic field, and other stimuli.[6–10] As biodegradable polymers/nanoparticles have an advantage in achieving long-term drug delivery when they degrade,[11] it is more attractive to introduce degradable property into the thermoresponsive PNIPAAm polymer system so that both stimuli-responsive and sustained drug delivery systems can be obtained.[12–15] Unfortunately, there is no report in the literature yet to introduce degradable components into thermoresponsive PNIPAAm micro- and nanogel systems.

In this study, we design and synthesize thermoresponsive and biodegradable nanogels by copolymerizing NIPAAm monomer with dextran-lactate-2-hydroxyethyl methacrylate (DEXlactate-HEMA)[16] macromer using the emulsion polymerization technique. Because of the existence of a hydrolyzable oligolactate spacer between each cross-linkable vinyl group and dextran backbone of DEXlactateHEMA, hydrolytically degradable cross-links can be formed within the nanogel particles, resulting in a hydrolytically degradable system. In addition, the hydrophobic lactateHEMA grafts and hydrophilic dextran backbone construct an amphiphilic macromer, which can perform as a surfactant to facilitate micelle formation during the emulsion polymerization; therefore, no extra surfactant is used for the reaction. In this study, we also use attenuate total reflection Fourier transform infrared spectroscopy (ATR-FTIR), light scattering (LS), transmission electron microscopy (TEM), and atomic force microscopy (AFM) techniques to thoroughly characterize the physicochemical properties of the developed nanogels, such as their chemical structure, size, and morphology changes with temperature and time.

It is noted here that from the simple chemistry point of view the current nanogels are chemically similar to the earlier reported hydrogels.[13] However, the nanoscale properties of these nanogels as well as many other nanoparticle systems cannot be simply extrapolated from the corresponding macroscopic properties. In addition, even though emulsion polymerization is one of common techniques for synthesizing nanoparticle/nanogel systems, it is not always successful for the synthesis because it depends on the reaction conditions, including monomer amounts and properties, surfactants, reaction temperature, and stirring speed. Especially, it is always challenging to synthesize stable nanosystems without surfactants. However, if surfactants are used for synthesizing nanosystems, the surfactant residues in the nanosystems are very difficult to be removed completely and later may cause toxicity when the obtained nanosystems are used for biomedical applications. In current work, we have developed multifunctional nanogel systems with both thermoresponsive and biodegradable properties through controlling the right composition and balance between the monomer/macromer without using surfactants. The nanogel materials themselves are not only novel but also have strong significance in biomedical applications.

* Corresponding author: e-mail tlowe@psu.edu; Ph 717-531-8602; Fax 717-531-4464.
[†] Department of Surgery.
[‡] Biomaterials and Bionanotechnology Summer Institute.
[||] Department of Biochemistry and Molecular Biology.
[§] Department of Bioengineering.
[⊥] Department of Materials Science and Engineering.
[#] Current address: Zimmer, Inc., 12024 Vista Parke Drive, Austin, TX 78726.

10.1021/ma800081g CCC: $40.75
Published on Web 11/04/2008

Scheme 1. Schematic Chemical Structure of DEXlactateHEMA (A) and NIPAAm-*co*-DEXlactateHEMA Nanogels (B)

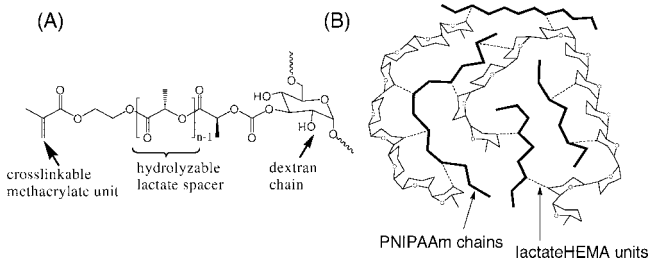

Experimental Section

Materials. Dextran (M_w = 15 000−20 000) was purchased from Polysciences, Inc., Warrington, PA. NIPAAm, 2-hydroxyl methacrylate (HEMA), 4-(*N,N*-diethylamino)pyridine (DMAP), *N,N′*-carbonyldiimidazole (CDI), L-lactide, stannous octoate, tetrahydrofuran (THF), dimethyl sulfoxide (DMSO), sodium dodecyl sulfate (SDS), and potassium persulfate (KPS) were obtained from Sigma-Aldrich, Inc., St. Louis, MO. All the chemicals were used as received. Deionized−distilled water was used in all the experiments.

Synthesis of DEXlactateHEMA Macromer. DEXlactateHEMA (Scheme 1) macromers were synthesized as described previously.[13] Three DEXlactateHEMA macromers were synthesized, with the average length of lactate spacer (DP_{AV}) equal to 3, 4, and 6 and theoretical degree of substitute (DS, amount of methacrylate groups per 100 dextran glucopyranose residues) equal to 17. Three steps were involved in the synthesis process.

Synthesis of HEMA-Lactate. To synthesize HEMA-lactate of DP_{AV} = 3, L-lactide (4.32 g, 30 mmol) and HEMA (3.90 g, 30 mmol) were reacted at 110 °C in a nitrogen atmosphere for 1 h in the presence of catalyst $SnOct_2$ (121.5 mg, 1 mol % with respect to HEMA). To separate HEMA-lactate product from unreacted HEMA, the cooled reaction mixture was dissolved in THF and precipitated in ice-cold water. The precipitate was dissolved in ethyl acetate and filtered to remove the remaining solids. The filtrate was dried over $MgSO_4$ and concentrated under reduced pressure to obtain purified HEMA-lactate with DP_{AV} = 3.

To synthesize HEMA-lactate of DP_{AV} = 4 or 6, 5 mmol of HEMA (0.65 g) was reacted with 10 or 15 mmol of lactate (1.44 or 2.16 g), respectively, for 1 h in the presence of catalyst $SnOct_2$ (20.25 mg, 1 mol % with respect to HEMA). On the basis of the previous work by van DijkWolthuis et al.,[16] when the molar ratio between the reactants lactate and HEMA was 2 or higher, no unreacted HEMA could be detected after the reaction; therefore, the HEMA-lactate product was used without further work-up procedure.

Synthesis of HEMA-LactateCI. CDI (0.81 g, 5 mmol) was dissolved in THF (20 mL) under nitrogen and reacted with equal molar amount of HEMA-lactate (1.73 g for DP_{AV} = 3, 2.09 g for DP_{AV} = 4, and 2.81 g for DP_{AV} = 6, based on theoretical calculation) at room temperature for 16 h. HEMA-lactateCI was concentrated by solvent evaporation under reduced pressure.

Synthesis of DEXlactateHEMA. Dextran (5 g, ∼30.86 mmol of glucopyranose residues) was dissolved in DMSO (45 mL) in a nitrogen atmosphere and then mixed with DMAP (1.0 g) and the concentrated HEMA-lactateCI (5 mmol). The mixture was stirred at room temperature for 4 days. The DEXlactateHEMA product was obtained after the reaction mixture was precipitated in large excess volume of cold dry 2-propanol, washed several times with 2-propanol, and dried in vacuum for 48 h. Assuming the reaction was complete with all of the HEMA-lactate grafted on dextran backbone, the theoretical DS for the final DEXlactateHEMA product was calculated to be ∼17 based on the molar feeding ratio between HEMA and glucopyranose residues.

Synthesis of Poly(NIPAAm-*co*-DEXlactateHEMA) Nanogels. P(NIPAAm-*co*-DEXlactateHEMA) nanogels were synthesized by emulsion polymerization without low molar mass surfactants in a 100 mL jacketed glass reactor equipped with a Teflon paddle for mechanical agitation. Briefly, DI water (57 mL) was placed in the reactor and stirred at 200 rpm at 70 °C with nitrogen bubbling for 30 min. Precursors DEXlactateHEMA and NIPAAm (900 mg in total) at selected weight ratios were dissolved in 1 mL of DI water and added into the reactor sequentially. The mixture was stirred for 15 min before KPS (36 mg) dissolved in 1 mL of DI water was added dropwise to initiate the polymerization. The reaction was allowed to proceed for 4 h. The obtained emulsion was cooled down to room temperature and dialyzed against large (10-fold) volume of DI water for 4 h using 50 kDa molecular cutoff cellulose dialysis tubes. The reason to use short 4 h for the dialysis was to limit the nanogel degradation during the dialysis process. The purified nanogel product was then dried by lyophilization for 48 h. The yield was above 85%.

For the later infrared characterization of the chemical structure of the nanogels, we have also synthesized homogeneous PNIPAAm latex as a control. The PNIPAAm latex was synthesized following almost the same procedure for the nanogels, except that 20 mg of SDS was added into the reaction as a surfactant before NIPAAm (900 mg) monomer was added, and no DEXlactateHEMA was used in the reaction.

Characterization. *Infrared Spectroscopy.* An attenuated total reflection (Pike Technologies, Madison, WI) Fourier transform infrared spectroscope (Thermo Nicolet Avetar 370, Madison, WI) (ATR-FTIR) was used to obtain IR spectra of samples including synthesized nanogels and nanogel solutions in PBS (pH 7.4) at 5 $mg \cdot mL^{-1}$ at selected degradation time points. A small amount of dry nanogels dissolved in DI H_2O or nanogel degradation solutions were cast on the ZnSe crystal and dried by air blowing. IR spectra were recorded in the range of 4000−650 cm^{-1} wavenumber.

Light Scattering. An ALV light scattering instrument capable of simultaneous static and dynamic light scattering (SLS and DLS) measurements was used. This instrument is equipped with an ALV-CGS-8F compact goniometer system, an ALV-5000/EPP multiple tau real-time correlator, and an ALV-5000/E/WIN software (ALV, Germany). The light source was JDS Uniphase helium/neon laser (633 nm, 35 mW, Manteca, CA). The nanogels' apparent average hydrodynamic radii at 90° scattering angle (R_h) in filtered PBS (pH 7.4) at a concentration of 200 $\mu g \cdot mL^{-1}$ were measured with gradually increasing temperature from 25 to 45 °C, and oscillating temperature between 25 and 37 °C for five cycles within 8 h, by using the ALV DLS technique. The sample solutions were stabilized for 10/20 min after temperature was gradually increased/oscillated to the next one. Autocorrelation functions of nanogel solutions at 90° scattering angle were collected three times every 10 min at each studied temperature. The data were fitted using a Cumulants method to derive apparent R_h of the nanogels, and the CONTIN program (a Laplace inverse program) was used to analyze the R_h distribution of the nanogels. The R_h was reported as mean ± standard deviation (SD). The LCSTs of the nanogels were defined as the initial break points of R_h−temperature curves.

SLS measurements were performed on studying the chemical and physical structure changes of the nanogels during the degradation at both 25 and 37 °C. The average intensities and intensity−time correlations of the scattered lights from the nanogels in filtered PBS (pH 7.4) solutions at concentrations c = 0.4, 0.8, 1, 1.6, and 2 mg mL^{-1} were collected from angle 20° to 40° with a 1° interval and then from angle 40° to 90° with a 5° interval. At each angle, each measurement was conducted for 60 s and repeated twice. For SLS studies, the measured average scattering intensity of PBS (pH 7.4) at each concentration and each angle was subtracted from that of the nanogels. The result was then normalized using the scattering intensity of a reference solvent (toluene) to obtain the Rayleigh ratio $R_\theta(q)$ as a function of scattering vector q, where $q = (4\pi n/\lambda_0)\sin(\theta/2)$, where n is the refractive index of the solvent, λ_0 is the wavelength of the incident beam in vacuo, and θ is the scattering angle. Data were plotted in the Berry format $[Kc/R_\theta(q)]^{1/2}$ vs $q^2 + kc$ and fitted by a polynomial of third order of q^2 and first order of c, due to the curvature of the plots.[17−19] $[Kc/R_\theta(q)]^{1/2}$ was extrapolated to zero concentration and plotted in the Holtzer form $q/[R_\theta(q)/Kc]_{c\to 0}$ against q. The linear mass density M_L, molar mass

Table 1. Nanogel Compositions

sample ID	NIPAAm:DEXlactateHEMA mass feeding ratio	DP_{AV} of DEXlactateHEMA[a]	theoretical number of NIPAAm units between cross-links
N8/1_6	8:1	6	101–122
N8/1_4	8:1	4	91–112
N8/1_3	8:1	3	86–107
N6/3_3	6:3	3	21–27

[a] For all the DEXlactateHEMA macromers, DS = 17.

per unit length, was calculated from the plateau at large q of the Holtzer plots:[18–23]

$$M_L = \frac{1}{\pi}\left[\frac{qR_\theta(q)}{Kc}\right]_{\text{plateau}} \quad (1)$$

Transmission Electron Microscopy (TEM). TEM images were acquired on a Philips 420, tungsten-based TEM (Philips Electron Optics, Eindhoven, The Netherlands) with an accelerating voltage of 120 keV at a point to point resolution 0.34 nm, a magnification of 800 000×, and a slight defocus to enhance contrast. Samples were prepared by suspending nanogels in ethanol solvent; then a couple of drops of the suspension were cast on a continuous carbon-coated 200 mesh copper grid and dried in the air. The Image J program was used to calculate the average size of the nanogels. A total of 30 nanogels in the TEM image were analyzed, and the data were reported as mean ± standard error (SE).

Atomic Force Microscopy (AFM). A Digital Instruments Nanoscope IIIa (Veeco Instruments Inc., Santa Barbara, CA) was used to study the size change of the synthesized nanogels with degradation. Dried nanogels were dissolved in pH 10 DI water at 200 μg mL^{-1}, and the obtained solution was incubated at 25 °C for 5 weeks. The 5-week-old nanogel solution (pH 10) or freshly prepared nanogel in water solution at 200 $\mu g \cdot mL^{-1}$ was diluted 20 times, deposited on freshly cleaved mica surface, and dried at room temperature. AFM images were obtained in tapping mode and analyzed by using Nanoscope imaging program. A total of 110 nanogels in a 256 × 256 μm area of height images were used in the analysis, and the diameter, height, and volume of the nanogels were calculated and reported as mean ± standard error (SE). Diameter and height were obtained by sectioning individual nanogels. The volume of the nanogels was estimated using the values of diameter and height and assuming an oblate hemispheroidal geometry. Differences between the nanogel sizes at the two time points were statistically analyzed using one-way analysis of variance (ANOVA). A statistically significant difference was reported if $p < 0.02$ or less.

Results and Discussion

Nanogel Synthesis. The chemical structure of the synthesized nanogels is sketched in Scheme 1. The novel material design allows the following three parameters to be easily adjusted during synthesis to obtain nanogels with a variety of properties: (a) DP_{AV} of DEXlactateHEMA macromer, the average number of hydrolyzable repeating lactyl unit in the lactate spacer (n in Scheme 1), which determines the degradation speed. An increased n usually leads to a slower degradation. (b) DS of DEXlactateHEMA macromer, the average amount of cross-linkable methacrylate groups per 100 dextran glucopyranose residues, which directly controls the cross-linking density of the hydrogels, thereby influencing their swelling property and degradation speed. (c)Feeding ratio between NIPAAm and DEXlactateHEMA for nanogel synthesis, which affects the network cross-linking density, thermosensitivity, and hydrophilic/hydrophobic balance of the hydrogels.

In this paper we focus on synthesizing a series of nanogels with different DP_{AV} and feeding ratios between NIPAAm and DEXlactateHEMA by emulsion polymerization without low molar mass surfactant. The detailed synthesis conditions of the nanogels are listed in Table 1. The ATR-FTIR spectra of nanogels N8/1_3 and N6/3_3, homogeneous PNIPAAm latex and DEXlactateHEMA macromer, are presented in Figure 1. The two nanogels contain characteristic peaks from both PNIPAAm and DEXlactateHEMA macromer, namely, the C═O stretching (1750 cm^{-1}) from the ester groups of lactate spacers, amide I and II (at ~1650 and ~1540 cm^{-1}), and divided bands of symmetric C−H bending from the $-CH(CH_3)_2$ group (1388 and 1371 cm^{-1}) attributed to PNIPAAm and C−OH stretching (~1010 cm^{-1}) due to the abundant hydroxyl groups of dextran backbone. Figure 1 also demonstrates that the relative intensities of the characteristic peaks of DEXlactateHEMA (C═O stretching at 1750 cm^{-1} and C−OH stretching at ~1010 cm^{-1}) to those of PNIPAAm (amide II at ~1540 cm^{-1}) in nanogel N6/3_3 are higher than those in nanogel N8/1_3. These results suggest that the nanogel syntheses were successful with chemical composition of the nanogels corresponding well with the monomer/macromer feeding ratios.

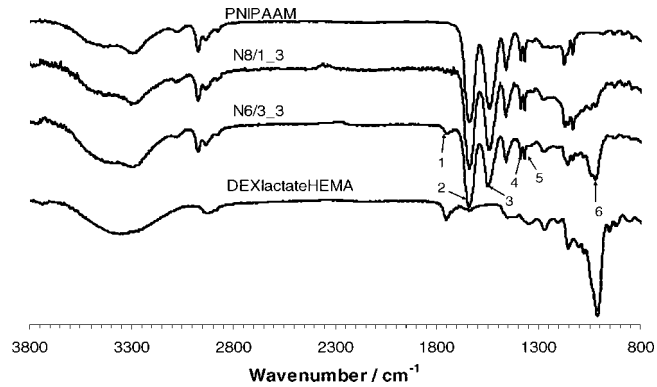

Figure 1. IR spectra of PNIPAAm latex, nanogels N8/1_3 and N6/3_3, and DEXlactateHEMA macromer. Peak 1: ester C═O stretching; peak 2: amide I; peak 3: amide II; peaks 4 and 5: C−H bending from $-CH(CH_3)_2$; peak 6: C−OH stretching.

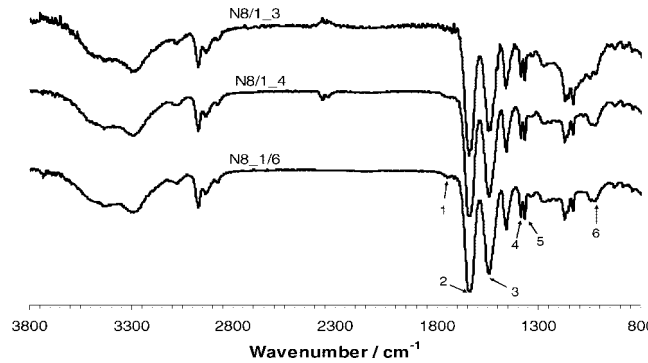

Figure 2. IR spectra of nanogels N8/1_3, N8/1_4, and N8/1_6. Peaks are the same as in Figure 1.

The ATR-FTIR spectra of nanogels N8/1_3, N8/1_4, and N8/1_6 are presented in Figure 2. The three nanogels have the same mass feeding ratio between NIPAAm and DEXlactateHEMA, but different lengths of lactate spacer (DP_{AV} = 3, 4, and 6). Figure 2 demonstrates that the relative FTIR peak intensity at 1750 cm^{-1} (C═O stretching of the ester linkage from lactate

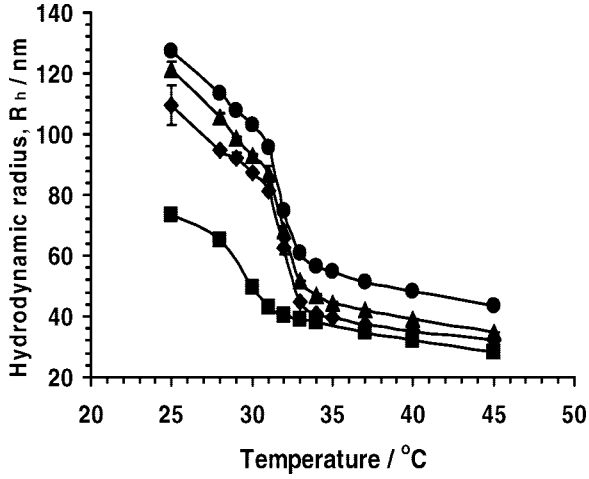

Figure 3. Hydrodynamic radii of the nanogels at 200 μg/mL in PBS (pH 7.4) measured by DLS at angle 90°: N8/1_3 (●), N8/1_4 (▲), N8/1_6 (♦), and N6/3_3 (■). Results represent the mean ±SD of three measurements. The nanogel solution was equilibrated for 10 min at each temperature.

spacers) to that at ~1010 cm^{-1} (C−OH stretching of dextran) increases in the order of nanogel N8/1_3 < N8/1_4 < N8/1_6. These results suggest that the nanogel syntheses were successful with chemical composition of the nanogels corresponding well with the lengths of lactate spacer.

Thermoresponsive Properties of Nanogels. Figure 3 shows that the synthesized four nanogels are thermoresponsive, evidenced by the decrease of hydrodynamic radii at angle 90° (R_h) with increasing temperature, which is similar to the swelling/deswelling behavior of the corresponding macroscopic hydrogels made of the same feeding components.[13] The radius decrease at elevated temperature is due to the increased hydrophobicity of the PNIPAAm segments, which leads to the collapse of polymer chains and the shrinkage of the gel network. All three nanogels N8/1_3, N8/1_4, and N8/1_6 show a gradual and continuous volume phase transition in the temperature range of 31−33 °C and a LCST at ~32 °C. The hydrodynamic radii of these three nanogels decrease in the order of nanogel N8/1_3 < N8/1_4 < N8/1_6 throughout the whole temperature range, indicating that the increase of DP_{AV}, the length of lactate spacers, leads to higher hydrophobicity and smaller size of the nanogels. On the other hand, with the same DP_{AV}, when the weight feeding ratio of NIPAAm/DEXlactateHEMA is changed from 8/1 to 6/3, significantly reduced nanogel sizes, much less dramatic thermoresponsive transition, and lower LCST are observed in nanogel N6/3_3 compared to those in nanogel N8/1_3. The reason may be because the nanogel 6/3 contains a less amount of thermoresponsive PNIPAAm component and a higher amount of cross-linkable and hydrophobic HEMAlactate grafts than the nanogel 8/1. It is worthy of mention that the nanogel 6/3 also contains more hydrophilic dextran component than the nanogel 8/1; however, the hydrophobic effects of the HEMAlactate grafts outperform the opposite hydrophilic effects of the hydrophilic dextran component on the overall thermoresponsive properties of the nanogels. CONTIN analysis demonstrates that all the four nanogels have monomodal particle size distributions at temperatures both below and above the LCST, as representatively shown with nanogel N8/1_3 in Figure 4. We have also measured the hydrodynamic radii of all the four types of nanogels against temperature at angles 45° and 145° and obtained temperature-dependent size trends similar to those at the angle 90° described above (data not shown), confirming that the nanogels are indeed thermoresponsive.

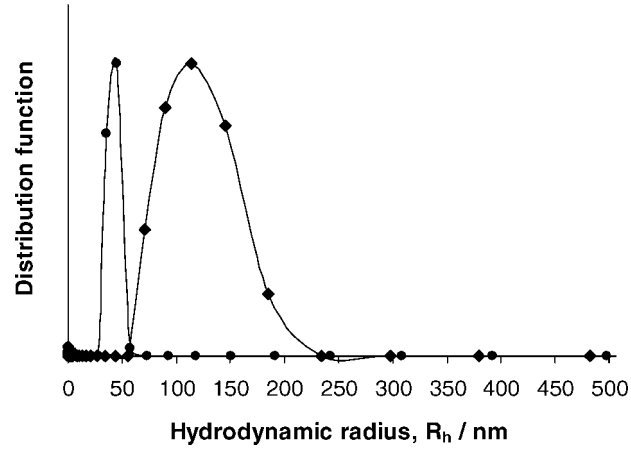

Figure 4. Hydrodynamic radius distribution of nanogel N8/1_3 at 25 (♦, below the LCST) and 37 °C (●, above the LCST), measured by DLS at angle 90°.

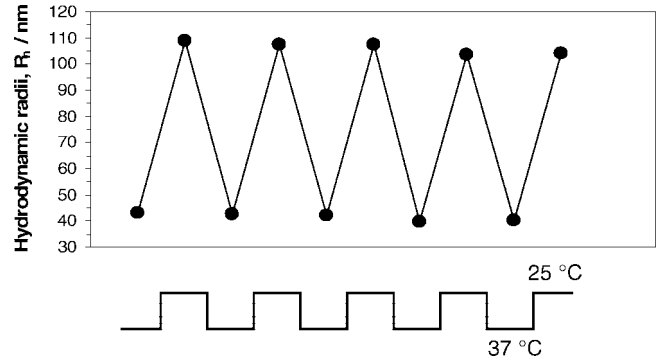

Figure 5. Hydrodynamic radius oscillation of nanogel N8/1_6 with temperature, measured by DLS at angle 90°. The nanogel solution was equilibrated for 10 min at each temperature.

To test the thermoreversibility of the synthesized nanogels, we measured the R_h of nanogel N8/1_6 at angle 90° when temperature was oscillated between 25 and 37 °C, below and above the LCST, for five cycles. The experiment was performed without interruption and finished within ~8 h to ensure that the effects of hydrolytic degradation on nanogel size change was minimal. Figure 5 demonstrates that the nanogel size change is completely reversible within the time and cycle ranges of this study. The cyclic size change corresponds to the cyclic swelling and shrinking of the nanogels at 25 and 37 °C, respectively. The reversible size change in Figure 5 indicates that the cyclic temperature change does not cause any permanent change of the morphology of the nanogels after the cyclic swelling and shrinking of the nanogels.

Hydrolytic Degradation of Nanogels. To study the degradation mechanisms of the nanogels, we used ATR-FTIR technique to measure the IR spectrum changes of the nanogel N6_3/3 after the nanogel was incubated in PBS (pH 7.4) at 5 mg·mL^{-1} at 25 °C, below the LCST, for 0, 3, 8, 13, and 21 days (Figure 6A) and at 37 °C, above the LCST, for 0, 3, 6, and 21 days (Figure 6B). The reason that much more concentrated nanogel solutions were used for ATR-FTIR studies than for the above DLS studies was to obtain clear IR spectra. In Figure 6, it can be clearly seen that at both 25 and 37 °C the intensity of ester C═O stretching at ~1750 cm^{-1} decreases with time, and carboxylate C═O stretching band at ~1710 cm^{-1} appears on day 3's IR spectrum and its intensity increases with time. In addition, the carboxylate C═O stretching peak at ~1710 cm^{-1} also becomes wider and turns into a shoulder-like peak of strong amide I band at ~1650 cm^{-1} with time. Figure 6 also reveals

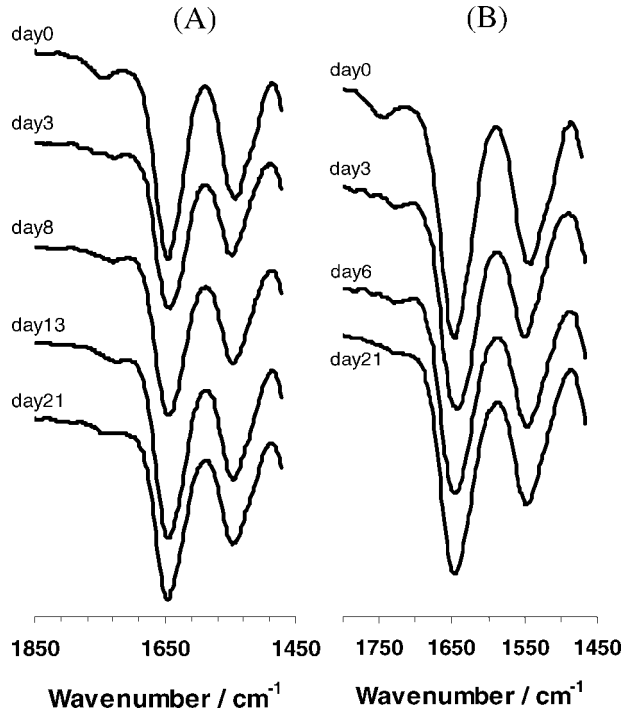

Figure 6. IR spectra change of nanogel N6/3_3 during degradation in PBS (pH 7.4) at 5 mg mL^{-1} at (A) 25 °C and (B) 37 °C.

that the most significant change in IR spectra occurs during the beginning 3 days. These results suggest that during the incubation of the nanogel N6_3/3 in PBS (pH 7.4) at both 25 and 37 °C the ester linkages of the oligolactate spacers are hydrolyzed, producing carboxylic acid and alcohol. The carboxylic acid exists in the form of carboxylate salt in PBS (pH 7.4) and has C═O stretching band at ~1710 cm^{-1}. It is also noted here that the FTIR peak intensities at ~1750 cm^{-1} normalized by those at ~1660 cm^{-1} (amide C═O stretching of PNIPAAM, relatively stable) at 25 °C at day 3 and 21 are weaker than those at 37 °C, indicating that the nanogel N6_3/3 degrades faster at 25 °C below the LCST than 37 °C above the LCST. This degradation trend is in agreement with the previous report on other thermoresponsive and hydrolytically degradable nanoparticle sytems.[14] Since the IR peaks of ester C═O stretching at ~1750 cm^{-1} of the nanogels N8/1_3, N8/1_4, and N8/1_6 were weak due to limit amount of oligolactate present in the nanogels, we did not perform time-dependent IR measurements for these three nanogels in PBS (pH 7.4).

Size and Morphology Changes of Nanogels with Degradation. Both TEM and AFM techniques were used to investigate the size and morphology changes of the nanogel N6_3/3 when the nanogel degraded in water. The TEM image of the nanogel in Figure 7 depicts that the nanogel is nanosized with an average diameter of 27.2 ± 1.2 nm at initial time. The weak contrast in the TEM image may be due to the noncrystalline nature of the nanogel.

Representative AFM height images of the nanogel N6_3/3 before and after degradation in pH 10 water at 25 °C for 5 weeks are shown in Figure 8. Before further discussion, we want to point out that since it is well known that polyesters degrade faster in basic solution than in pure water and in the previous section we demonstrate that the nanogel N6_3/3 degrades with time and faster at 25 °C than 37 °C, we chose the "pH 10, 25 °C and 5 weeks" degradation condition to obtain a sample with significant degradation characteristics for the AFM studies. The AFM images in Figure 8 clearly illustrate that the average size of the nanogel at day 0 is bigger than at 5 weeks later. After

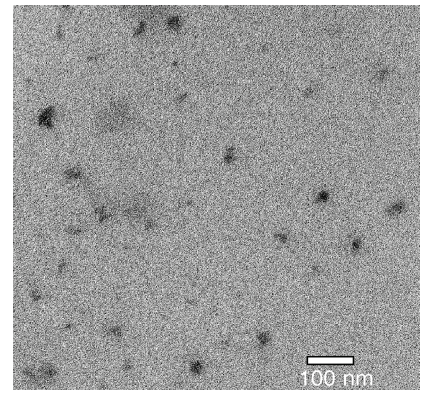

Figure 7. TEM image of the N6/3_3 nanogel in dry state. The average size of the nanogel is 27.2 ± 1.2 nm; mean ±SE of 30 particles.

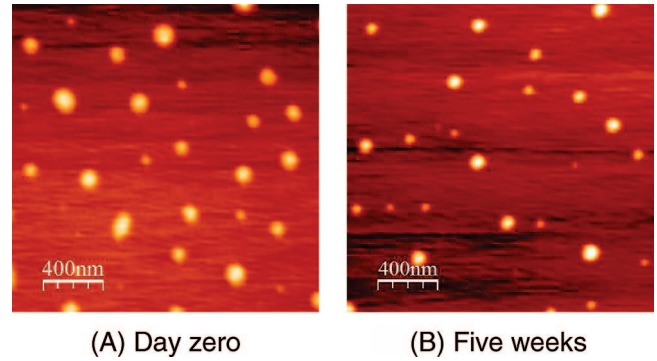

Figure 8. Representative AFM height images of the nanogel N6/3_3 (A) before and (B) after 5 weeks of degradation. The yellow and dark red colors correspond to the nanogel and mica surface, respectively.

quantification of 110 nanogel particles in Figure 8, the average diameter and height of the nanogel N6_3/3 are calculated to be 132 ± 31 nm and 3.24 ± 0.80 nm, respectively, at day 0 and 113 ± 24 nm and 4.04 ± 1.22 nm, respectively, at 5 weeks. These results demonstrate that the nanogel's height is always much smaller than the diameter, suggesting that the nanogels are flat on the mica surface probably due to the amorphous nature of the nanogel. With assumption that the nanogel N6_3/3 has an oblate hemispheroidal geometry on the mica surface and use of the above calculated values of diameter and height, the volume of the nanogel N6_3/3 was calculated to be 34.1 ± 2.1 and 28.0 ± 1.4 μm^3 at day 0 and 5 weeks, respectively. These two volumes correspond to sphere particles in suspension state with diameters of 38.3 ± 0.8 and 36.7 ± 0.6 nm, respectively. It is noted here that the sphere diameter of the nanogel N6_3/3 at day 0 obtained from the AFM calculation (38.3 ± 0.8 nm) is higher than that obtained from the TEM measurement (27.2 ± 1.2 nm). The reason may be due to the fact that the TEM image was obtained by suspending the nanogel in poor solvent ethanol, which causes the nanogel to shrink and attain smaller size than under the air-drying process for the AFM image.

Figure 9A−C demonstrates that the diameter, height, and volume of the nanogel N6_3/3 statistically significantly ($p < 0.005$) decreases 14%, increases 25%, and decreases 18%, respectively, after 5 weeks of degradation. The 18% decrease of the volume strongly suggests that the nanogel is hydrolytically degradable, and its size decreases with degradation. As height/diameter ratio gives useful information on the stiffness of nanoparticles,[24] we further calculate that the height/diameter ratios of the nanogel N6_3/3 at day 0 and 5 weeks which are $2.47 \times 10^{-2} \pm 0.04 \times 10^{-2}$ and $3.75 \times 10^{-2} \pm 0.14 \times 10^{-2}$, respectively. The ca. 52% increase of the height/diameter ratio after the nanogel degrades for 5 weeks (Figure 9D) suggests

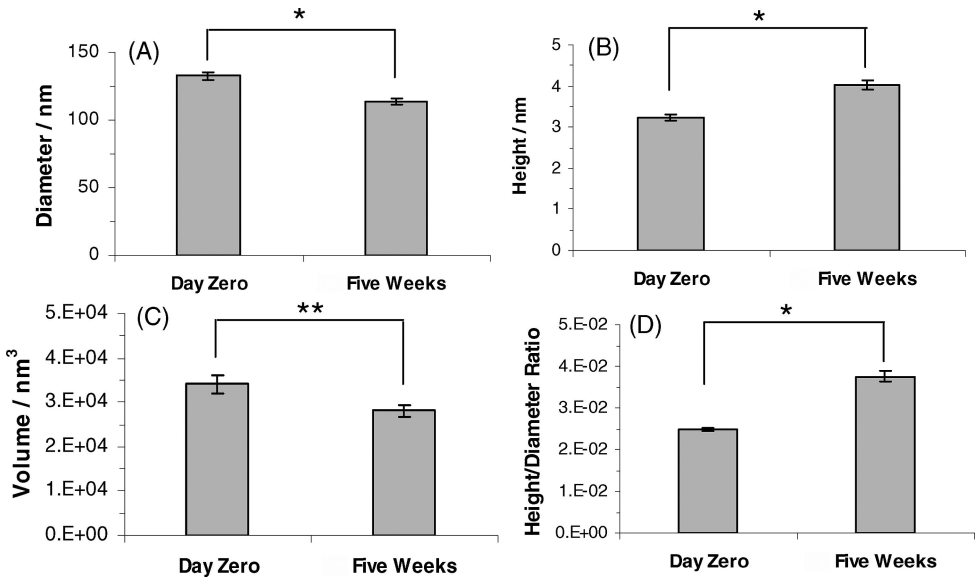

Figure 9. Calculated (A) diameter, (B) height, and (C) volume of the N6/3_3 nanogels before and after 5 weeks of degradation extracted from the AFM images. Results represent the mean ± SE of 110 measurements. *: $p < 1 \times 10^{-6}$. **: $p < 0.02$.

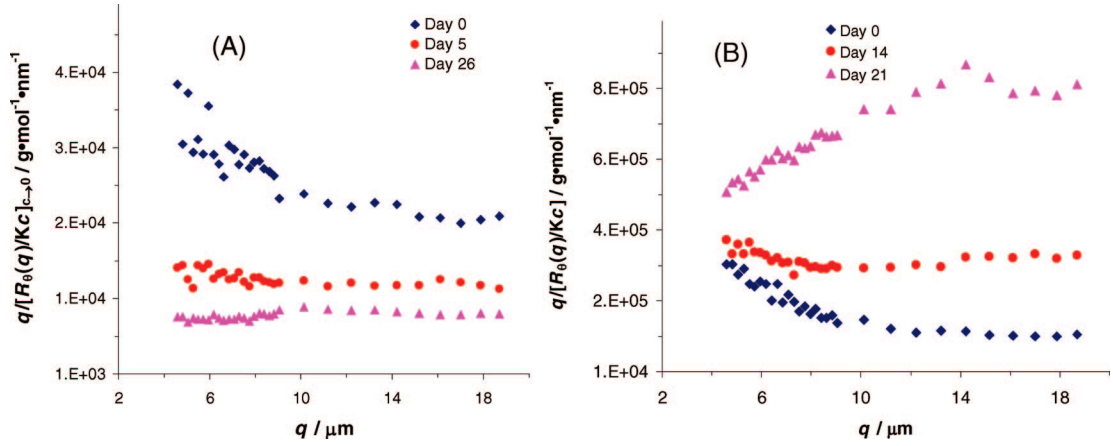

Figure 10. Holtzer plots of static light scattering data of nanogel N6/3_3 after degradation in PBS (pH = 7.4) at (A) 25 °C for 0, 5, and 26 days and at (B) 37 °C for 0, 14, and 21 days.

that the nanogels become stiffer with degradation. The reason may be that the nanogel becomes more hydrophobic as a result of the loss of hydrophilic dextran from the nanogels with degradation.[13]

The Holtzer plot is well-known to give detailed information on wormlike structure as well as rod structure. It shows a plateau at large q for rod structure, and the plateau height gives the linear mass density which depends on chemical structure alone but not chain length polydispersity.[20,21] The Holtzer plots of the nanogel N6_3/3 at both 25 and 37 °C in Figure 10 show the left upward curvatures at small q become less pronounced with time at both 25 and 37 °C, suggesting that the nanogel N6_3/3 in PBS (pH 7.4) changes from coil-like (hydrophilic, loose) to more rod-like (hydrophobic, stiff) structure with degradation. On the basis of the plateau heights at large q in Figure 10 and eq 1, we calculate that the linear mass density M_L of the nanogel N6_3/3 is (22 ± 3) × 10^3, (13 ± 1) × 10^3, and (9 ± 1) × 10^3 g•mol^{-1}•nm^{-1} after the nanogel degrades for 0, 5, and 26 days, respectively, at 25 °C, and (11 ± 2) × 10^4, (33 ± 5) × 10^4, and (80 ± 14) × 10^4 g•mol^{-1}•nm^{-1} after the nanogel degrades for 0, 14, and 21 days, respectively, at 37 °C. The decreasing/increasing M_L with time at 25/37 °C is more than likely because the nanogel degrades with time and becomes more and more hydrophobic with degradation at 37 °C.

Conclusions

A series of thermoresponsive and hydrolytically degradable nanogels were successfully synthesized by the emulsion polymerization technique without low molar mass surfactant through free radical polymerization of NIPAAm and DEXlactateHEMA (DP_{AV} = 3, 4, and 6; DS = 17), a cross-linkable and hydrolytically degradable dextran derivative at mass feeding ratios: NIPAAm/DEXlactateHEMA = 8:1 and 6:3 (w/w). The chemical structures of the nanogels were confirmed by ATR-FTIR measurements. The thermoresponsive properties of the synthesized nanogels in PBS (pH 7.4) were studied by measuring the nanogels' R_h in PBS (pH 7.4) as a function of temperature and angle using DLS. All the four synthesized nanogels N8/1_3, N8/1_4, N8/1_6, and N6/3_3 decreased their R_h with increasing temperature and showed a LCST at ~32 °C, a typical phase transition temperature of PNIPAAm-based polymer.

ATR-FTIR measurements showed that the peak intensity of the nanogel N6/3_3 at ~1750 cm^{-1} decreased with time at both 25 °C (below the LCST) and 37 °C (above the LCST), suggesting that the nanogel N6/3_3 did degrade and the degradation mechanism was due to the hydrolytic degradation of its ester bonds. Both TEM and AFM measurements confirmed that the nanogel N6/3_3 is nanosized with a sphere diameter

smaller than ca. 50 nm. AFM image analysis further revealed that the nanogel N6/3_3 became smaller and more rigid with degradation in pH 10 water at 25 °C, as evidenced by the decrease of its volume and the increase of its height/diameter ratio, respectively. Holtzer plots further proved that the nanogel N6/3_3 changed from more coil-like structure to more rod-like structure with degradation at both 25 and 37 °C, temperatures below and above the LCST, respectively.

Future nanogel characterization work will include use of flow field flow fractionation technique to study the polydispersity of the nanogels and simultaneous static and dynamic light scattering to investigate the changes of the molecular weight, radius of gyration, density, and translational hydrodynamic radius of the nanogels with degradation. Current ongoing research encompasses incorporation of drugs into the nanogels during the emulsion polymerization synthesis procedure, studies of the effects of the chemical composition of the nanogels on the drug release kinetics, and evaluations of the in vitro and in vivo biosafety, bioavailability, and bioefficacy of the nanogel/drug systems.

Acknowledgment. The authors are grateful to the Whitaker Foundation and the Penn State Surgery Feasibility Grant for financial support. We also thank Dr. Li-Chong Xu and Dr. Eun Seok Gil, Department of Surgery, Pennsylvania State University, for helping with the AFM data.

References and Notes

(1) Allen, T. M.; Cullis, P. R. *Science* **2004**, *303*, 1818–1822.
(2) Pelton, R. *Adv. Colloid Interface Sci.* **2000**, *85*, 1–33.
(3) Kuckling, D.; Vo, C. D.; Adler, H. J. P.; Volkel, A.; Colfen, H. *Macromolecules* **2006**, *39*, 15851591.
(4) Lowe, T. L.; Benhaddou, M.; Tenhu, H. *J. Polym. Sci., Part B: Polym. Phys.* **1998**, *36*, 2141–2152.
(5) Pelton, R. H.; Chibante, P. *Colloids Surf.* **1986**, *20*, 247–256.
(6) Ballauff, M.; Lu, Y. *Polymer* **2007**, *48*, 1815−1823.
(7) Lopez, V. C.; Hadgraft, J.; Snowden, M. J. *Int. J. Pharm.* **2005**, *292*, 137−147.
(8) Nolan, C. M.; Serpe, M. J.; Lyon, L. A. *Macromol. Symp.* **2005**, *227*, 285−294.
(9) Ozdemir, N.; Tuncel, A.; Kang, M. C.; Denkbas, E. B. *J. Nanosci. Nanotechnol.* **2006**, *6*, 2804−2810.
(10) Rubio-Retama, J.; Zafeiropoulos, N. E.; Serafinelli, C.; Rojas-Reyna, R.; Voit, B.; Cabarcos, E. L.; Stamm, M. *Langmuir* **2007**, *23*, 10280−10285.
(11) Van Thienen, T. G.; Lucas, B.; Flesch, F. M.; van Nostrum, C. F.; Demeester, J.; De Smedt, S. C. *Macromolecules* **2005**, *38*, 8503–8511.
(12) Huang, X.; Nayak, B. R.; Lowe, T. L. *J. Polym. Sci., Part A: Polym. Chem.* **2004**, *42*, 5054–5066.
(13) Huang, X.; Lowe, T. L. *Biomacromolecules* **2005**, *6*, 2131–2139.
(14) Kim, Y. S.; Gil, E. S.; Lowe, T. L. *Macromolecules* **2006**, *39*, 7805–7811.
(15) Stover, T. C.; Kim, Y. S.; Lowe, T. L.; Kester, M. *Biomaterials* **2008**, *29*, 359–369.
(16) vanDijkWolthuis, W. N. E.; Tsang, S. K. Y.; KettenesvandenBosch, J. J.; Hennink, W. E. *Polymer* **1997**, *38*, 6235–6242.
(17) Andersson, M.; Wittgren, B.; Wahlund, K. G. *Anal. Chem.* **2003**, *75*, 4279–4291.
(18) Burchard, W. *Makromol. Chem., Macromol. Symp.* **1988**, *18*, 1–35.
(19) Schmidt, M. Simultaneous static and dynamic light scattering application to polymer structure analysis. In *Dynamic Light Scattering—The Method and Some Applications*; Brown, W., Ed.; Oxford Science Publications: Oxford, 1993; pp 373−381.
(20) Savin, G.; Burchard, W. *Macromolecules* **2004**, *37*, 3005–3017.
(21) Denkinger, P.; Burchard, W. *J. Polym. Sci., Part B: Polym. Phys.* **1991**, *29*, 589–600.
(22) Burchard, W.; Frank, M.; Michel, E. *Ber. Bunsen-Ges.* **1996**, *100*, 807–814.
(23) Aberle, T.; Burchard, W.; Galinsky, G.; Hanselmann, R.; Klingler, R. W.; Michel, E. *Macromol. Symp.* **1997**, *120*, 47–63.
(24) Kazakov, S.; Kaholek, M.; Kudasheva, D.; Teraoka, I.; Cowman, M. K.; Levon, K. *Langmuir* **2003**, *19*, 8086–8093.

MA800081G